Eur. Phys. J. D **17**, 79–83 (2001)

THE EUROPEAN PHYSICAL JOURNAL D

EDP Sciences

Luminescence characteristics of ultraviolet upconversion from Er^{3+}:YAG crystal by Ar^{+} laser (488 nm) excitation

H. Xu[a], Z. Dai, and Z. Jiang

Department of physics, Jilin University, ChangChun 130023, P.R. China

Received 20 March 2001 and Received in final form 11 July 2001

Abstract. Ultraviolet and violet upconversion signals at 271 nm, 317 nm, 381 nm and 407 nm were observed when an erbium-doped YAG crystal was pumped by an Ar^{+} laser (488 nm). The dependence of intensity of luminescence emitting from the $^4S_{3/2}$ state and the $^2P_{3/2}$ state on pump power (I) was experimentally investigated. Changes from I^1 down to $I^{1/2}$ for the $^4S_{3/2}$ state and from I^2 down to I^1 for the $^2P_{3/2}$ state were observed. The upconversion mechanism was discussed by means of the rate equations. It appears that energy-transfer upconversion (ETU) is a dominant process for the Er^{3+}:YAG crystal used in our experiment.

PACS. 42.65.Ky Harmonic generation, frequency conversion

1 Introduction

Recently, there has been an intense interest in the study of the energy upconversion phenomena of trivalent Erbium ion-doped crystals and fibers [1–3]. Several upconversion materials, such as, Er^{3+}:BaF_2, Er^{3+}:$YAlO_3$ and Er^{3+}:Ba_2YCl_7, have been identified, and the upconversion mechanisms have been discussed as well [4,5]. However, Er^{3+}-doped yttrium aluminum garnet, to our knowledge, has not been reported in detail concerning the ultraviolet upconversion phenomena. The crystal host ($Y_3Al_5O_{12}$) commonly referred to as YAG, has a cubic space-group symmetry O_h^{10} and is superior in terms of hardness and thermal conductivity. The Er^{3+} ions substitute Y^{3+} ions on the dodecahedral sites having D_2 symmetry [6]. Previous studies in Er^{3+}:YAG were concentrated on luminescence properties in the visible and infrared regions [7–9]. The purpose of this paper is to investigate luminescent characteristics of ultraviolet upconversion in this crystal. The two most common excitation processes that lead to emission from energy states higher than the terminating state of the first pump-absorption step are pump excited-state absorption (ESA) and energy-transfer upconversion (ETU) [5,10].

Here we report on the generation of ultraviolet and violet upconversion signals under 488-nm Ar^{+} laser excitation. For the interpretation of short-wavelength luminescence, we measured the dependence of intensity of luminescence emitting from the $^4S_{3/2}$ state and the $^2P_{3/2}$ state on pump power. The rate equations for the ESA and ETU processes were used to provide a framework for discussing the upconversion mechanism.

[a] e-mail: jzk@mail.jlu.edu.cn

2 Experiment and results

The Er^{3+}:YAG (30 mol%) sample grown by a conventional Czochralski technique in Changchun Institute of Applied Chemistry of China, has a size of $1.0 \times 0.5 \times 0.4$ cm^3. All experiments were performed at room temperature. The absorption spectrum of the crystal (see Fig. 1) was measured by a Perkin-Elmer Lambda-9 UV-visible-near-infrared spectrophotometer with a resolution of 0.2 nm. According to the wavelengths of absorption peaks and the energy level data given in reference [11], we made the energy-level diagram of Er^{3+} ion in the crystal (see Fig. 2).

For the upconversion investigation, the sample was pumped by an argon-ion laser (Spectra Physics 171) in a single-line mode (488 nm) with the beam chopped by a light chopper (EG&G 9479). A 488 nm narrow band filter was used to avoid the light from the Ar^{+} laser plasma lines. The fluorescence was collected in a direction perpendicular to the incident beam by a 4-cm-diameter, 10-cm-focal-length quartz lens placed at the entrance slit of a 1-m double grating monochromator (Jobin-Yvon U-1000), which had been calibrated by a Hg lamp. The exit slit of the monochromator was equipped with a photomultiplier tube (Hamamatsu R955). The signals from photomultiplier tube were sensed by a boxcar integrator (EG&G Princeton Applied Research Model 4400 Signal detection and analysis system) and recorded by a computer. A standard lamp was used to calibrate the spectra-response curve of this system.

When the sample was pumped by a 488-nm Ar^{+} laser which is resonant with $^4F_{7/2}$ state, we observed the upconversion signals at 271 nm, 317 nm, 381 nm, 407 nm as shown in Figure 3. In addition, the long-wavelength luminescence signals (Fig. 4) at 543 nm and 656 nm

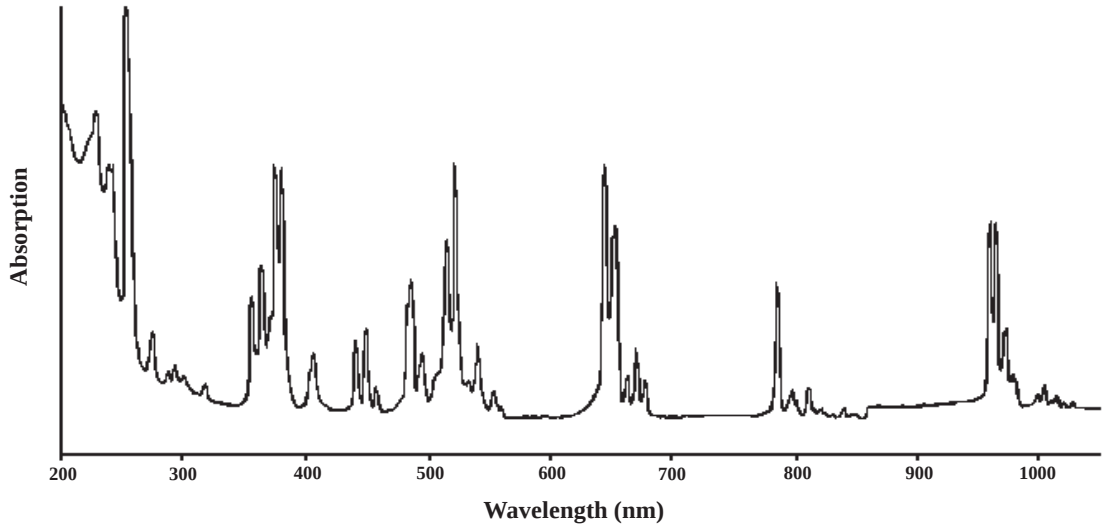

Fig. 1. Absorption spectrum of the Er^{3+}:YAG crystal containing 30 at% Er^{3+} ion.

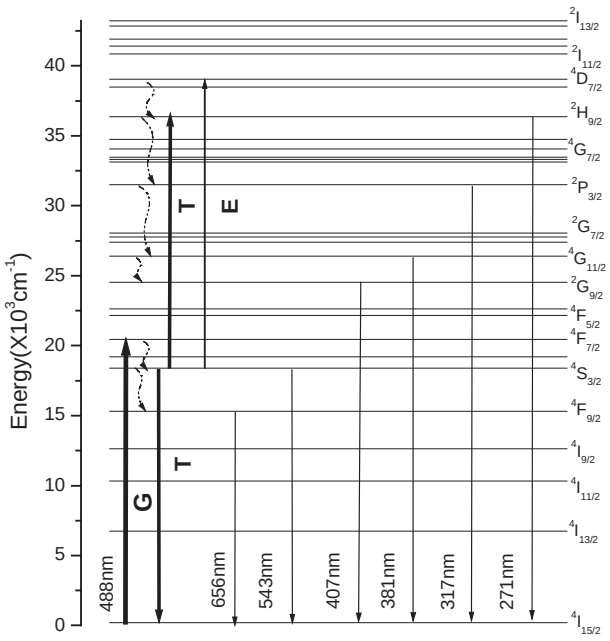

Fig. 2. Energy level diagram of Er^{3+}:YAG showing related transitions. G: ground-state absorption; T: energy transfer; E: excited state absorption; wavy arrows: multiphonon relaxation; the other straight arrows: fluorescence emission.

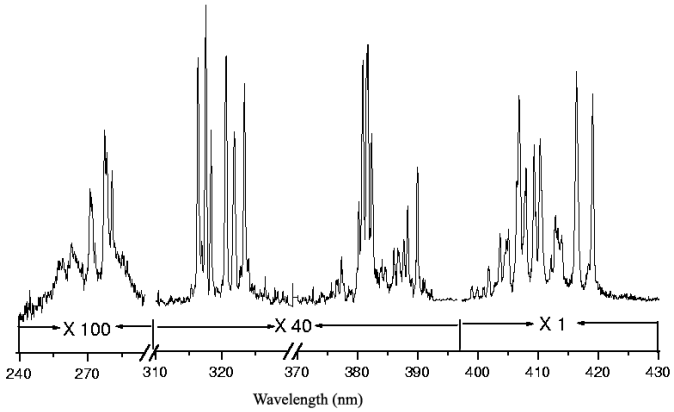

Fig. 3. Upconversion fluorescence spectrum of Er^{3+}:YAG under 488 nm excitation. The numbers below the spectrum are the intensity amplification multiples of the corresponding spectrum.

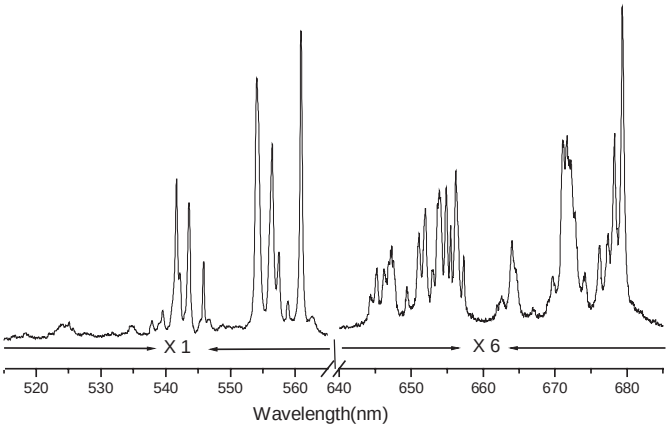

Fig. 4. Downconversion fluorescence spectrum of Er^{3+}:YAG. The numbers below the spectrum are the intensity amplification multiples of the corresponding spectrum.

were also observed. According to the energy-level data given in reference [11], we made the assignment of luminescence transitions: 271 nm ($^2H_{9/2} \rightarrow {}^4I_{15/2}$), 317 nm ($^2P_{3/2} \rightarrow {}^4I_{15/2}$), 381 nm ($^4G_{11/2} \rightarrow {}^4I_{15/2}$), 407 nm ($^2G_{9/2} \rightarrow {}^4I_{15/2}$), 543 nm ($^4S_{3/2} \rightarrow {}^4I_{15/2}$) and 656 nm ($^4F_{9/2} \rightarrow {}^4I_{15/2}$). For the signal at 381 nm, it is also possible from the transition ($^2H_{9/2} \rightarrow {}^4I_{11/2}$), but the intensity of the luminescence emitting from the $^2H_{9/2}$ state to the $^4I_{11/2}$ state is weaker as that of the luminescence (271 nm) emitting from $^2H_{9/2}$ to the ground state, because their transition probabilities (not shown) are found

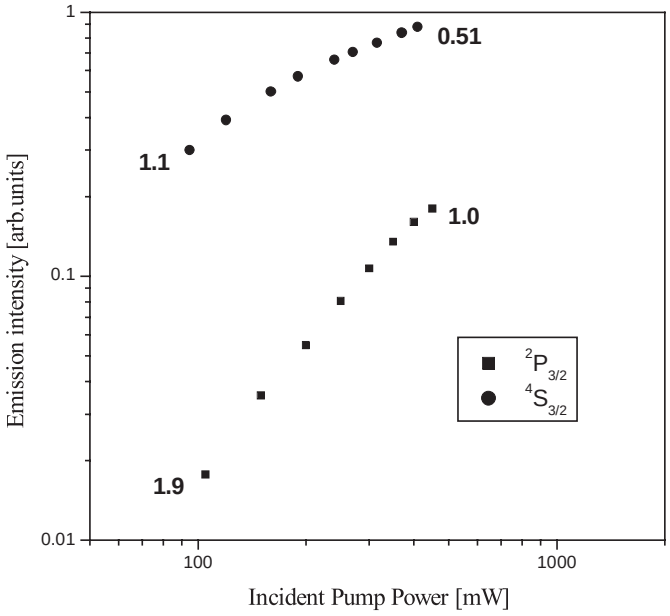

Fig. 5. Measured emission intensities from the $^2P_{3/2}$ and $^4S_{3/2}$ levels at 317 nm and 543 nm, respectively, in YAG:30%Er^{3+} *vs.* pump power. The numbers denote the slopes in double-logarithmic representation at low and high pump power, respectively.

to be comparable. Therefore, the luminescence at 381 nm emitting from the $^2P_{3/2}$ state to the ground state is dominant. For the signal at 407 nm, the transitions from the $^2H_{9/2}$ state to the $^4I_{9/2}$ state and from the $^2P_{3/2}$ state to the $^4I_{13/2}$ state are also possible. According to the calculations of transition probabilities and the similar analysis as 381 nm, the luminescence at 407 nm dominantly come from the transition from the $^2G_{9/2}$ state to the ground state. In addition, luminescence from other excited states is too small to be observed due to their small energy gap to the next lower-lying levels and the large phonon energy (850 cm^{-1}) in this crystal [12]. The corresponding transitions of the observed luminescence are indicated in Figure 2.

The luminescence observed at wavelengths longer than 488 nm (see Fig. 4) is due to the emissions from the $^4S_{3/2}$ and $^4F_{9/2}$ states, which were populated by multiphonon relaxation from the $^4F_{7/2}$ state.

The dependence of intensity of luminescence from the $^4S_{3/2}$ and $^2P_{3/2}$ states on pump power was measured by inserting different neutral density filters in the pump beam. The results are shown in Figure 5 in double logarithmic scale.

3 Discussion

To understand the physical mechanism responsible for the observations described above, we introduced the rate equations to analyze the ESA and ETU processes. When the Er^{3+} ions in the crystal are excited by ground-state absorption (GSA) at 488 nm into the $^4F_{7/2}$ level, subsequent rapid multiphonon relaxation leads to the population of the $^4S_{3/2}$ state, where an upconversion process due to ESA and/or ETU may occur as depicted in Figure 2.

At first, we demonstrate the relevant effect of the ESA process on luminescence intensity *versus* pump power. The ESA process takes place when some of Er^{3+} ions in exited state $^4S_{3/2}$ absorb 488 nm photons to populate $^4D_{7/2}$. Subsequent nonradiative relaxation from the $^4D_{7/2}$ state populates the $^2H_{9/2}$, $^2P_{3/2}$, $^4G_{11/2}$ and $^2G_{9/2}$ states resulting in the upconversion luminescence. The rate equations for the ESA process are given by

$$\frac{\mathrm{d}N_2}{\mathrm{d}t} = \mu N_1 \frac{I\sigma_{1l}}{h\nu} - N_2 \frac{I\sigma_{2m}}{h\nu} - R_2 N_2 \quad (1)$$

$$\frac{\mathrm{d}N_3}{\mathrm{d}t} = \mu' N_2 \frac{I\sigma_{2m}}{h\nu} - R_3 N_3 \quad (2)$$

where subscripts 1, 2, 3 refer to the $^4I_{15/2}$, $^4S_{3/2}$ and $^2P_{3/2}$ states, respectively; N_i, R_i are the population density and decay rate of state i, respectively; $h\nu$ is the pump photon energy and I is the pump laser intensity; σ_{1l} is the absorption cross-section from $^4I_{15/2}$ to $^4F_{7/2}$ and σ_{2m} from $^4S_{3/2}$ to $^4D_{7/2}$; μ, μ' are the nonradiative relaxing percentage from upper states to the $^4S_{3/2}$ state and the $^2P_{3/2}$ state, respectively. Under the steady-state case, *i.e.*, $\mathrm{d}N/\mathrm{d}t = 0$, equations (1, 2) become

$$\mu N_1 \frac{I\sigma_{1l}}{h\nu} = N_2 \frac{I\sigma_{2m}}{h\nu} + R_2 N_2 \quad (3)$$

$$\mu' N_2 \frac{I\sigma_{2m}}{h\nu} = R_3 N_3. \quad (4)$$

From equations (3, 4), the relation between the population of the $^4S_{3/2}$, $^2P_{3/2}$ states and the incident laser power can be obtained by

$$N_2 = \frac{\mu N_1 I\sigma_{1l}}{I\sigma_{2m} + R_2 h\nu} = C_1 \frac{I}{I\sigma_{2m} + R_2 h\nu} \quad (5)$$

$$N_3 = \frac{\mu\mu' N_1 \sigma_{1l}\sigma_{2m} I^2}{h\nu R_3 (I\sigma_{2m} + R_2 h\nu)} = C_2 \frac{I^2}{I\sigma_{2m} + R_2 h\nu} \quad (6)$$

where C_1, C_2 are constants. From equations (5, 6), we can see that, if $I\sigma_{2m} \gg R_2 h\nu$, then $N_2 \propto I^0$ and $N_3 \propto I$, if $I\sigma_{2m} \ll Rh\nu$, then $N_3 \propto I^2$ and $N_2 \propto I$. The absorption cross-section σ_{2m} can be deduced by

$$\sigma_{2m} = \frac{h\nu B_{2m}}{c} g(\nu - \nu_0) \quad (7)$$

where ν is the transition frequency of the $^4S_{3/2}$ state to the $^2P_{3/2}$ state; $g(\nu - \nu_0)$ is the Voigt profile, which is a convolution of Lorentzian and Gaussian profiles; B_{2m} is the Einstein absorption coefficient, which has the form [13]

$$B_{2m} = \frac{\pi\chi(n)}{3\varepsilon_0\hbar^2} |M_{2m}|^2 \quad (8)$$

where $\chi(n)$ is the factor of refractive index under Lorentz-local-field correction for crystal, $|M_{2m}|^2$ is the electric dipole matrix element. The oscillator strength between two multiples can be calculated by Judd-Ofelt

theory [14,15]. In principle, the oscillator strength between individual Stark levels can also be approximately evaluated with complicated calculation by utilizing group-symmetry characteristics of Stark levels [16]. However, from our previous paper [16], we found that the dipole matrix elements related to every Stark level of a multiple state have the same orders of magnitude. Thus, $|M_{2m}|^2$ can be approximately calculated by taking the average of all the Stark levels of the $^4D_{7/2}$ state, *i.e.*

$$|M_{2m}|^2 = \frac{2}{2J+1}\frac{2}{2J'+1}e^2 \times \sum_{t=2,4,6} \Omega_\lambda \left| \left\langle 4f^N(\alpha SL)J \| U^\lambda \| 4f^N(\alpha' S'L')J' \right\rangle \right|^2 \quad (9)$$

where J, J' are the quantum numbers of angular momentum of the $^4S_{3/2}$ state and $^4D_{7/2}$ state, respectively. The factors 2 in equation (9) arose from the Kramers degenerate of the Stark levels of Er^{3+}. The reduced matrix element U^λ and the phenomenological intensity parameter Ω_λ used in equation (9) were obtained from references [17,18]. Inserting all data into equation (7), we obtained the cross-section $\sigma_{2m} = 3.583 \times 10^{-21}$ cm^2. From the experimental lifetime value of the $^4S_{3/2}$ level [19], the decay rate R_2 was obtained as $R_2 = 2 \times 10^6$ s^{-1}. Under our regions of laser power used here (see Fig. 5), it is found that $I\sigma_{2m}$ (about 10^{-16} J s^{-1}) $\ll h\nu R_2$ (about 10^{-13} J s^{-1}). If the ESA process is dominant, the luminescence intensity of $^4S_{3/2}$ state should be proportional to N_2 and therefore to the intensity I. Similarly, for the $^2P_{3/2}$ state, the luminescence intensity should be proportional to N_3 and to I^2. Since the experimental results do not show this kind of dependences, we conclude that ESA is not the dominant process.

Therefore, we have considered the ETU upconversion process. ETU takes place between two ions in the $^4S_{3/2}$ state to produce an ion in the $^2H_{9/2}$ state and another one in the ground state. Accordingly, the rate equations have the forms

$$\frac{dN_2}{dt} = \mu N_1 \frac{I\sigma_{1l}}{h\nu} - 2WN_2^2 - R_2N_2 \quad (10)$$

$$\frac{dN_3}{dt} = \mu' WN_2^2 - R_3N_3 \quad (11)$$

where W is cross relaxation rate. All other symbols have the same meanings as for ESA. Under steady-state excitation, this relations lead to

$$\mu N_1 \frac{I\sigma_{1l}}{h\nu} = 2WN_2^2 + R_2N_2 \quad (12)$$

$$\mu' WN_2^2 = R_3N_3. \quad (13)$$

If linear decay (term R_2N_2) is the dominant depletion mechanism of $^4S_{3/2}$ level, the upconversion term $2WN_2^2$ can be neglected in equation (12). It follows from equations (12, 13) that $N_3 \propto N_2^2 \propto I^2$. In contrast, if the upconversion term is dominant, then $N_3 \propto N_2^2 \propto I$. As a result, with increasing pump power, the upconversion term $2WN_2^2$ gets more important and the slope of the upconversion luminescence curve changes from 2 to 1, whereas that of the downconversion luminescence changes from 1 to 0.5. From the experimental results (Fig. 5), it can be seen that the slope of curve for the $^2P_{3/2}$ state changes from 1.9 to 1.0, while that of $^4S_{3/2}$ changes from 1.1 to 0.51. Therefore the theoretical analysis based on the ETU upconversion mechanism is in good agreement with the experimental results. This is contrary to what was observed in several Er^{3+}-doped compounds, such as, Er^{3+}:BaF_2 (2 mol%) and Er^{3+}:ZBLAN fiber [1,2]. Upon 488 nm excitation, in fiber sample the luminescence at 320 nm and 402 nm exhibited quadratic dependence on the incident laser power [2] and in BaF_2 sample the lifetime curve of the upconversion luminescence suggests the absence of the energy transfer [1]. Consequently the ESA process is the dominant mechanism in upconverting the signals in these two compounds.

As well-known, ETU is an interionic process whose probability depends on the distance between the participating ions and temperature [7,9,20]. Under our experimental condition (300 K and 30 at%), it is reasonable that ETU is a dominant upconversion process.

4 Summary

The ultraviolet and violet upconversion luminescence in Er^{3+}:YAG under 488-nm Ar^+ laser excitation has been observed. In order to understand the mechanism of the luminescence generation, the dependence of luminescence intensities *versus* pump power were measured. Two possible upconversion processes were analyzed based on the use of rate equations. It is demonstrated that ETU is a dominant process for the sample used.

The YAG crystal is an excellent host material for upconversion luminescence compared with other compounds, such as $RbGd_2X_7$ (X = Cl, Br), K_2LaX_5 (X = Cl, Br), and $Cs_3Lu_2X_9$ (X = Cl, Br, I), which are all very sensitive to moisture. It is also interesting to investigate the ultraviolet upconversion luminescence for many applications. In the present paper, we have reported a preliminary study of ultraviolet upconversion in Er^{3+}:YAG. It is necessary to carry out experimental measurements with different Er^{3+} ion concentration and temperature and to compare the efficiency of upconversion with other Er^{3+} doped compounds in the future.

The authors are grateful to the financial support from the National Natural Science Foundation of China (No. 10074020) and the Young Teacher Foundation of Jilin University (No. 2000A05).

References

1. D.N. Patel, R.B. Reddy, S.K. Nash-Stevenson, Appl. Opt. **37**, 7805 (1998).
2. C.L. Pope, R.B. Reddy, S.K. Nash-Stevenson, Opt. Lett. **22**, 295 (1997).

3. R. Scheps, IEEE J. Quant. Electron. **30**, 2914 (1994).
4. T. Riedener, P. Egger, J. Hulliger, H.U. Güdel, Phys. Rev. B **56**, 1800 (1997).
5. M. Pollnau, D.R. Gamelin, S.R. Lüthi, H.U. Güdel, M.P. Hehlen, Phys. Rev. B **61**, 3337 (2000).
6. J.B. Gruber, M.E. Hills, R.M. Macfarlane, C.A. Morrison, G.A. Turner, Chem. Phys. **134**, 241 (1989).
7. W.Q. Shi, M. Bass, M. Birnbaum, J. Opt. Soc. Am. B **6**, 23 (1989).
8. S. Georgescu, V. Lupei, A. Lupei, V.I. Zhekov, T.M. Murina, M.I. Studenkin, Opt. Commun. **81**, 186 (1991).
9. A. Lupei, V. Lupei, S. Georgescu, I. Ursu, V.I. Zhekov, T.M. Murina, A.M. Prokhorov, Phys. Rev. B **41**, 10923 (1990).
10. S.R. Lüthi, M. Pollnau, H.U. Güdel, M.P. Hehlen, Phys. Rev. B **60**, 162 (1999).
11. J.B. Gruber, J.R. Quagliano, M.F. Reid, F.S. Richardson, M.E. Hills, M.D. Seltzer, S.B. Stevens, C.A. Morrison, T.H. Allik, Phys. Rev. B **48**, 15561 (1993).
12. T.T. Basiev, Y.V. Orlovskii, K.K. Pukhov, V.B. Sigachev, M.E. Doroshenko, I.N. Vorobev, J. Lumin. **68**, 241 (1996).
13. R. Loudon, *The quantum theory of Light*, 2nd edn. (Clarendon press, Oxford, 1983).
14. B.R. Judd, Phys. Rev. **127**, 750 (1962).
15. G.S. Ofelt, J. Chem. Phys. **37**, 511 (1962).
16. Z.W. Dai, J.Y. Liu, S.Y. Zhang, Phys. Lett. A **265**, 233 (2000).
17. A.A. Kaminskii, V.S. Mironov, A. Kornienko, S.N. Bagaev, G. Boulon, A. Brenier, B.D. Bartolo, Phys. Stat. Sol. (a) **151**, 231 (1995).
18. Q.Y. Wang, S.Y. Zhang, Y.Q. Jia, J. Alloys Comp. **202**, 1 (1993).
19. V.I. Zhekov, T.M. Murina, A.M. Prokhorov, M.I. Studenikin, S. Georgescu, V. Lupei, I. Ursu, Sov. J. Quant. Electron. **16**, 274 (1986).
20. D.L. Dexter, J. Chem. Phys. **21**, 836 (1953).